



# CAPILLARY PHENOMENA IN LIQUID COMPOSITE MOULDING

Véronique Michaud\*, Markus Nordlund\*, T. Staffan Lundström\*\*, Jan-Anders E. Månson\*  
[V.Michaud]: veronique.michaud@epfl.ch

\*Laboratoire de Technologie des Composites et Polymères (LTC), Ecole Polytechnique  
Fédérale de Lausanne (EPFL), CH 1015 Lausanne

\*\*Division of Fluid Mechanics, Luleå University of Technology  
SE-971 87 Luleå, Sweden

**Keywords:** *capillary effects, liquid composite moulding, unsaturated flow, wetting*

## Abstract

*In liquid composite moulding, capillary phenomena take place as the fibre/air interface is progressively replaced by the fibre/resin interface. These effects are often neglected when computing the flow front progression into the fibre preform, because the surface tension of the resins is low. However, these are recognized to exert an influence on the final void content of the part. In this article, we present experimental results from unidirectional infiltration of an epoxy resin under constant flow rate into non-crimp fabrics. The inlet pressure rise is shown to deviate from linearity, indicating a progressive saturation. A multiphase flow approach is proposed to model infiltration, assuming saturation curves and relative permeability dependence on saturation based on soil science literature. Numerical results using a FEM code show trends that are in good qualitative agreement with experimental results. The interest and validity of this approach is then discussed.*

## 1 Introduction

During filling of a textile fabric in the Liquid Composite Moulding process, air/fibre interfaces are progressively replaced by resin/fibre interfaces at the flow front. Across this flow front, a pressure difference is created by the difference in surface tension between the phases [1]. If the resin progresses with a fully saturated flow front (often called "slug-flow"), the pressure difference across

the front is the capillary pressure drop  $\Delta P_\gamma$ , enhancing flow if it is negative, and working against it if positive. It is defined as the work needed to replace air by resin within a unit volume of a porous medium :

$$\Delta P_\gamma = -S_f \gamma_{SL} \cos(\theta_D), \quad (1)$$

where  $\theta_D$  is the dynamic contact angle to the fibres,  $S_f$  is the area of fibres per unit volume of matrix and  $\gamma_{SL}$  the surface tension of the resin to air. In Liquid Composite Moulding literature, capillary effects have been generally neglected, because the surface tension of most resins is very low, and applied pressures rather high. It is shown however that these effects play an important role in void formation during infiltration at low pressure injections [2, 3]. Several methods have been proposed to measure the capillary pressure drop assuming a fully saturated flow, using infiltration at constant flow rate or applied pressure [4-6]. For viscous resins, constant flow rate is preferred, as the dynamic contact angle may depend on the infiltrating resin velocity [4]. The inlet pressure should then increase linearly with time, and the intercept of this curve with the time axis provide the value of the capillary pressure drop. Significant deviations from the slug-flow behaviour have however been found in many practical cases, in particular when measuring the inlet pressure change with time during a constant flow rate injection [7-12]. From these observations, the pressure rise is often observed to be slower depending on the type of fabric and its compaction level. Apart from potential deviations due to experimental issues, such as a

curved flow front or race-tracking, it is generally accepted that these are due to the occurrence of unsaturated flow. In many practical cases, the fabric shows a distribution of pore sizes (often bi-modal). Multiphase flow takes place, and capillary phenomena manifest themselves by a progressive saturation of the fabric. Several methods have been proposed to address this issue: (i) take into account the multi-scale nature of the reinforcement, and model infiltration at two levels, the intra-tow and inter-tow regions [8, 9, 11, 12, 14]. In general, flow is assumed to first take place in between the fabric tows, and to slowly penetrate the tows behind the infiltration front. This implicitly assumes that the fluid does not wet the fabric, or that flow is perpendicular to the tows. A sink term is introduced in the models, providing fairly good agreement when adjusting the saturation rate, and for transverse infiltration [8, 13, 14, 15]. (ii) Another approach is to use the multiphase flow description used in soil science and reservoir engineering, introducing a saturation curve which is a function of the applied pressure, as well as a relative permeability term also varying with saturation [15-17]. This second approach has so far not been used for Liquid Composite Moulding processes.

In this work, we present experimental results on the inlet pressure rise during infiltration of a glass fabric by epoxy resin under constant flow-rate conditions. The validity of the saturated flow approach is discussed, and a multiphase flow description based on the second approach is proposed and discussed. Both cases of wetting or non-wetting conditions are investigated.

## 2 Theory

### 2.1 Saturated flow

For saturated flow into a porous medium under constant applied flow-rate, the inlet pressure  $P_{in}$  is written as:

$$(P_{in} - P_{atm}) = \frac{Q^2 \eta}{A^2 K (1 - V_f)} t + \Delta P_\gamma \quad (2)$$

where  $K$  is the permeability of the fibre bed,  $\eta$  the viscosity of the fluid,  $P_{atm}$  the atmospheric pressure,  $Q$ , the flow rate,  $A$  the cross sectional area of the fibre bed,  $V_f$  the fibre volume fraction and  $t$ , time. Equation (2) indicates that  $\Delta P_\gamma$  can theoretically be determined from a single experiment of the inlet

pressure difference measurement, which is linear in time, as represented in Figure 1 (in the graph, for illustration,  $\Delta P_\gamma = 1$  or  $-1$  in arbitrary units). This simplicity is beneficial, since it is not necessary to track the flow front position in order to determine  $\Delta P_\gamma$  as required for the constant pressure method presented in [4].

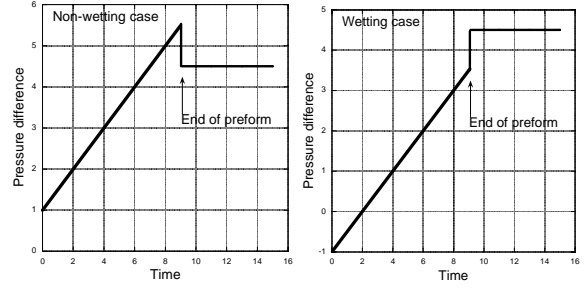


Fig. 1. Theoretical inlet pressure versus time for a constant flow rate experiment, for a non-wetting and a wetting case.

### 2.2 Unsaturated flow

If the unsaturated region is large, a multiphase flow approach needs to be used, and the inlet pressure curve, for a constant flow rate injection, will not be linear. By similarity with soil mechanics, we define the saturation  $S$  of fluid phase  $\alpha$  as:

$$S_\alpha = \frac{V_\alpha}{(1 - V_f)}, \quad (3)$$

with  $V_\alpha$  as the volume fraction of fluid phase  $\alpha$ . When the preform is empty of fluid phase  $\alpha$ , the saturation  $S_\alpha$  is equal to 0, and when it is fully filled  $S_\alpha$  equals 1; all governing equations are then those for saturated flow. It is generally assumed that the densities of liquid and solid phases are constant; in most cases of non-reactive infiltration, this is a reasonable assumption.

Mass conservation equation is written for the fluid phases, as:

$$\frac{\partial \left( (1 - V_f) S_\alpha \right)}{\partial t} + \nabla \cdot q_\alpha = 0, \quad (4)$$

where  $q_\alpha$  is the specific discharge for phase  $\alpha$  [18]. Assuming that no momentum transfer occurs between the phases and that both the inertial effects and the resistance to the flow from the viscous shear

inside each fluid are negligible, the momentum balance equations for the flow is generally written using Darcy's law:

$$q_\alpha = -\frac{Kk_{r,\alpha}}{\eta_\alpha}\nabla p_\alpha, \quad (5)$$

where  $K$  is the saturated permeability,  $k_{r,\alpha}$  the relative permeability scalar (a function of  $S_\alpha$  and  $V_f$ ),  $\eta_\alpha$  the viscosity of phase  $\alpha$  and  $p_\alpha$  the pressure in the phase  $\alpha$  [18]. Equation (5) is valid provided the relevant Reynolds number, defined in relation to the average fluid velocity and the pore diameter, is less than about one: for all but some metal infiltration processes, this will be the case. Initial and boundary conditions valid for each case complete the definition of this non-linear problem. The solution for constant flow rate injection requires the use of a numerical tool; in the present case Comsol Multiphysics 3.3 with the Earth Science module was used.

The main characteristics of the fibre preform and of the fluid necessary to obtain a solution of the problem are:

- (i): the viscosity  $\eta$  assumed to be constant over the time of the flow front progression.
- (ii) the dependence of the saturation  $S_\alpha$  on the local pressure  $P$ , a function which is governed by capillarity,
- (iii) the permeability  $K$  and  $k_{r,\alpha}$ , which depends on the local value of the solid volume fraction  $V_f$  as well as on the saturation  $S_\alpha$ .

The functions (ii) and (iii) are not known a priori, and need to be determined experimentally as indicated in Soil Science literature [18-22]. In the present case, to explore the practical use of this approach, we assumed the values of these functions, based on the soil science literature, for two extreme cases: (1) the resin fully wets the fabric, so the resin is the wetting phase, and air is the non-wetting phase, (ii) the resin does not wet the fabric, so the resin is the non-wetting phase. In practice, it was shown for this type of epoxy that depending on the capillary number  $Ca = \eta u_{in}/(1-V_f)\gamma_L$  (with  $u_{in}$  the superficial velocity and  $\gamma_L$  the resin surface tension) the resin changes from a wetting phase to a non-wetting phase, as the contact angle increases [4]. In what follows, we will not take this into account, and assume that the saturation curves do not depend on the fluid velocity.

The curves for the fluid saturation and the relative permeability, in the case of non-wetting

resin injection, are based on the well known analytical van Genuchten equations [23] in the forms:

$$q_\alpha = -\frac{Kk_{r,\alpha}}{\eta_\alpha}\nabla p_\alpha, \quad (5)$$

$$S_w = \begin{cases} \frac{1}{(1 + |\beta H_p|^n)^{1/m}}, & H_p > 0 \\ 1, & H_p \leq 0 \end{cases}, \quad (6)$$

$$k_{r,w} = \begin{cases} S_w^l \left[ 1 - (1 - S_w^{1/m})^m \right]^2, & H_p > 0 \\ 1, & H_p \leq 0 \end{cases}, \quad (7)$$

$$S_{nw} = 1 - S_w, \quad (8)$$

$$k_{r,nw} = \begin{cases} (1 - S_w)^l \left( 1 - S_w^{1/m} \right)^{2m}, & H_p > 0 \\ 1, & H_p \leq 0 \end{cases}, \quad (9)$$

where the subindex  $w$  denotes the wetting air phase and  $nw$  the non-wetting ( $nw$ ) resin.  $H_p = (p_{nw} - p_w)/(\rho g)$ , is the capillary pressure head, with  $\rho$  the density of the resin and  $g$  the gravitational constant. The indices  $l=0.1$ ,  $n=2$ ,  $m=1-1/n$  and the parameter  $\beta=0.75$  are used in the present paper, resulting in saturation and relative permeability curves for the non-wetting resin injection as shown in Fig. 2. In the case when the injected resin is the wetting phase, the curves are mirrored around  $H_p=0$  and  $S_\alpha, k_{r,\alpha}=0.5$  and furthermore shifted with a bubbling pressure head  $H_b=5m$  to take the shapes shown in Fig. 3. The bubbling pressure head is the pressure head difference needed to be overcome for the resin to be injected. These curves are similar to the saturation curves found in [24,25] for typical glass fibre mats or fabrics and oil. Such curves were also measured for metal/ceramic systems [16, 17, 26].

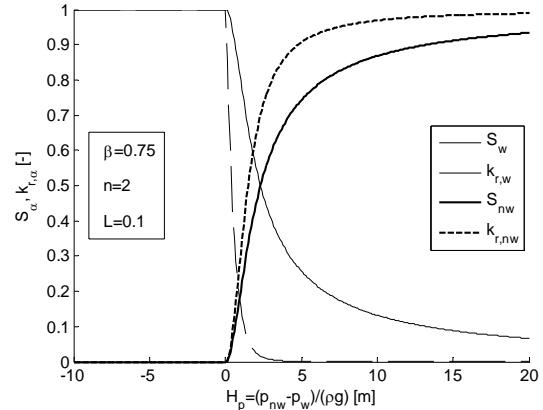


Fig. 2. Saturation curves and relative permeability curves in the case of a non-wetting resin and a wetting phase.

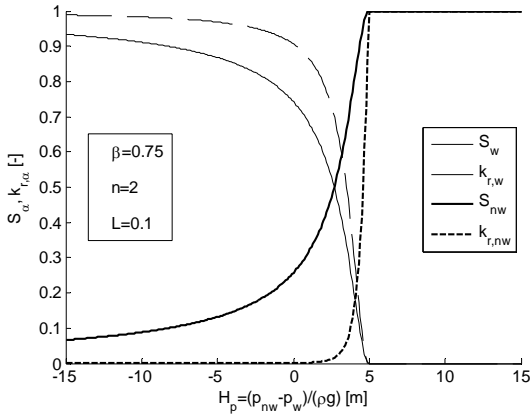


Fig. 3. Saturation curves and relative permeability curves in the case of a wetting resin and a non-wetting gas phase.

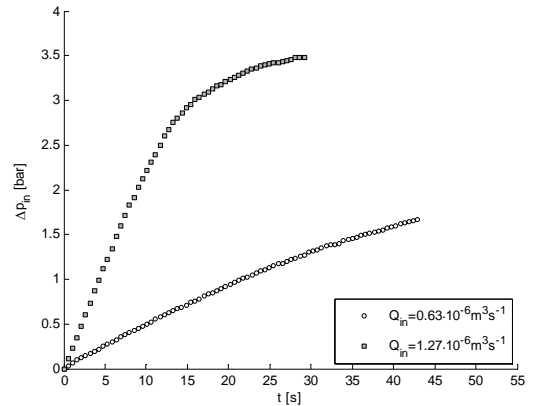


Fig. 4. Inlet pressure difference as a function of time, with the carbon fabric oriented at  $\pm 45^\circ$  and a constant flow-rate.

### 3 Materials and experiments

The resin was a commercial, thermoset two component system: Epikote 828LV epoxy resin from Shell and Shell Epikure DX 6514 hardener. The mixing ratio for this system was 100:17 parts by weight of base and hardener, respectively. The injection temperature was chosen to be  $80^\circ\text{C}$ , leading to a stable resin viscosity of about  $0.08 \text{ Pa}\cdot\text{s}$  during 3 minutes. The resin surface tension was  $\gamma_L = 32 \text{ mN/m}$

In a first series of experiments, 3 layers of a biaxial NCF fabrics [+45/-45] based on carbon fibres (T700 from Toray, woven by Saertex GMBH) were stacked in the mould to reach a fibre volume fraction of 47%, with a fabric size of  $0.152\text{m} \times 0.152\text{m} \times 1.1\text{mm}$  [4]. In another series, four layers of a biaxial [+45/-45] glass fibre NCF, DB810E05-A, from Devold AMT were stacked into the mould. The dimensions of the injected parts for the second series experiments were  $0.08 \text{ m} \times 0.08 \text{ m} \times 2 \text{ mm}$ , leading to  $V_f \approx 62\%$ . The mould was flat with a transparent glass top, and could be heated up to  $200^\circ\text{C}$ . In order to avoid flow racing at the sides of the fabric, the fabric lay-up was sealed on the sides. The constant flow rate was delivered with an Eldo-Mix 101 injection unit from Dopag AG (Cham, CH). The inlet pressure difference was measured with a pressure transducer with a sensitivity of  $0.1 \text{ kPa}$ , at the entrance of the mould.

### 4 Experimental Results

Several experiments were performed, with various flow-rates and a constant fabric orientation of [+45/-45] with respect to the flow. Fig. 3 presents typical curves of inlet pressure difference ( $P_{in} - P_{atm}$ ) as a function of time for two flow rates ( $Q \in [6.30 \cdot 10^{-7} \text{ } 1.27 \cdot 10^{-6}] \text{ m}^3 \text{ s}^{-1}$ ) for infiltration into the carbon fabric, corresponding to capillary number values of 0.0176 and 0.035, respectively [4]. The pressure behaviour follows the trend reported in many cases of NCF infiltration [7-12], the slope drooping with time.

For infiltration into the glass NCF fabric, typical set of pressure inlet curves for several experiments as a function of time are given in Figure 4 for two flow rates,  $Q \in [1.56 \cdot 10^{-7} \text{ } 2.21 \cdot 10^{-7}] \text{ m}^3 \text{ s}^{-1}$ , along with linear regression curves from the straight portion of the curves. In this case, the capillary numbers are about ten times lower, ranging from 0.004 to 0.006. The shape of the curve is different, and is similar to what was observed for low capillary numbers in [4]. Assuming a saturated flow approach, the capillary pressure drop can be estimated from the intersection of the linear regression of the pressure curve with the Pressure difference axis. This indicates that Fig. 4 would correspond to a non-wetting case, with a positive capillary pressure, and that Fig. 5 is typical of a wetting case. This approach however shows its limits: the linear region is sometimes rather narrow, and it is difficult to precisely determine in what time interval the linear regression should be performed. Also, the value of

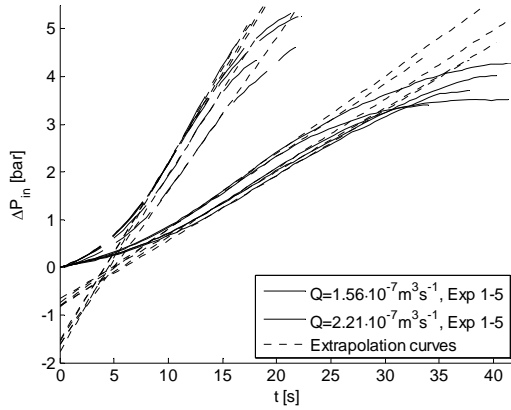


Fig. 5. Inlet pressure difference as a function of time for several experiments, with the glass fabric oriented at  $\pm 45^\circ$  and a constant flow-rate.

the slope may be modified by non-saturation, as the local permeability will vary with saturation in a non-linear manner. Extracting a permeability value from the value of the slopes at various times has been proposed by several authors [8, 9], but this averaged value is difficult to interpret, since permeability varies within the infiltrated length of the sample. A multiphase flow approach seems appropriate to analyze these curves.

## 5 Numerical Modelling

The unsaturated flow of resin in a one dimensional geometry extended between  $x=0.0\text{m}$  and  $x=0.1\text{m}$  was studied for both non-wetting and wetting resin injection for four injection velocities,  $u_{in} \in [2.0 \cdot 10^{-3}, 1.0 \cdot 10^{-3}, 5.0 \cdot 10^{-4}, 2.5 \cdot 10^{-4}] \text{ ms}^{-1}$ , corresponding to capillary numbers in the range 0.0125 - 0.0015. The permeability of the porous material was set to  $K=1.0 \cdot 10^{-11} \text{ m}^2$  and the fibre volume fraction to  $V_f=0.6$ , since these values are commonly found for textiles used in Liquid composite moulding processes. A finite element method with quadratic shape functions was used to solve for the pressure fields resulting from Equations (3)-(5) for both the resin and the air. The geometry was spatially discretized into three meshes with element lengths:  $h \in [1.0 \cdot 10^{-3}, 5.0 \cdot 10^{-4}, 2.5 \cdot 10^{-4}] \text{ m}$  (DOF 402, 802, 1602). The three discretizations are furthermore used to control the spatial discretization convergence. In order to solve the nonlinear system of equations, a differentiation formula was used, which resulted in an implicit time-stepping scheme for the solver. A combination of Newton iteration

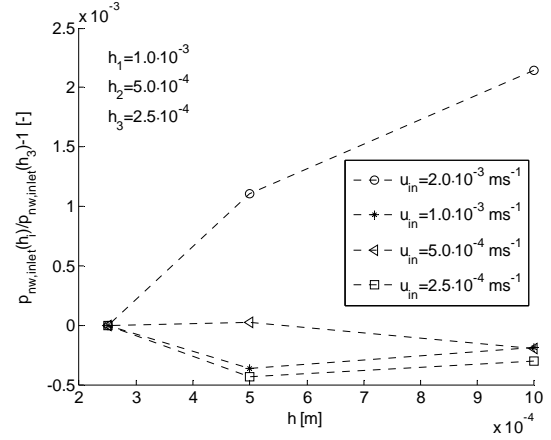


Fig. 6: Spatial discretization convergence for the inlet pressure difference after the resin is injected  $2 \cdot 10^{-3} \text{ m}$  into the geometry for all  $u_{in}$ .

for the nonlinear variable-order, variable step-size backward system and a COMSOL Multiphysics linear system solver for the resulting systems was used to solve for the pressure fields [27].

The viscosity and density were  $\eta_{resin}=0.1 \text{ Pas}$  and  $\rho_{resin}=1200 \text{ kgm}^{-3}$  for the resin and  $\eta_{air}=2.1 \cdot 10^{-5} \text{ Pas}$  and  $\rho_{air}=1.25 \text{ kgm}^{-3}$  for the air. The boundary conditions for the resin phase consisted of a fluid flux,  $u_{in}$ , at the inlet ( $x=0$ ) and a zero flux condition at the outlet ( $x=0.1$ ). For the air phase, a zero flux condition was applied at  $x=0$  and the pressure was set to zero at the outlet ( $x=0.1$ ). During constant flow rate injections of a fabric in a closed mould, resin is advancing through the inlet tubes at a constant speed pushing air through the dry fabric. Hence, the initial condition for the air pressure was calculated by Darcy's law for steady state flow of air through a dry fabric. The initial condition for the pressure of the resin was determined from the saturation curves, Fig. 2 and 3 for the case of a non-wetting resin and a wetting resin, respectively, to ensure that the initial saturation of the resin was close to zero in the domain.

## 6 Numerical Results for unsaturated flow

The values of the pressure difference at the inlet,  $p_{nw,inlet}$ , after the resin was injected  $2 \cdot 10^{-3} \text{ m}$  into the geometry was used to study the spatial discretization convergence. The values of the inlet pressure difference for the three meshes and the four inlet fluxes in Fig. 6 indicate that the spatial discretization error between the coarsest and finest

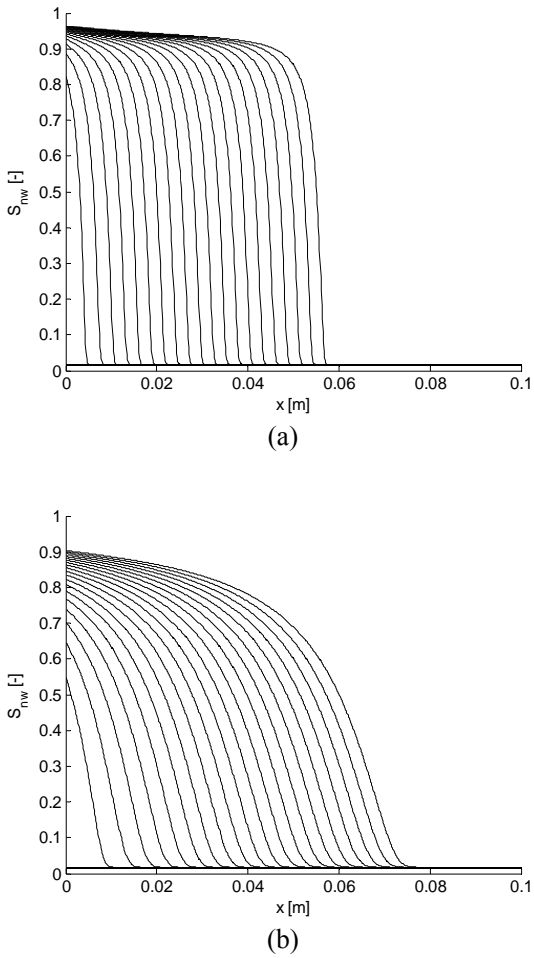


Fig. 7. Evolution of the non-wetting resin saturation with time for (a)  $u_{in}=2.0 \cdot 10^{-3} \text{ ms}^{-1}$ , up to 10s, and (b)  $u_{in}=2.5 \cdot 10^{-4} \text{ ms}^{-1}$ , up to 80s.

mesh was less than 0.2% for all flow conditions studied. Hence, the results for the finest meshes could be used with confidence for the analyses.

Saturation profiles for a non-wetting resin are given in Fig. 7 (a) and (b) as a function of position, for different values of time (time increments of 0.5 and 4 seconds in Fig. (a) and (b), respectively) and two flow rates. As expected, saturation progressively increases with time as the flow front progresses, and the saturation gradient is less for a low flow rate.

Fig. 8 plots the saturation profiles along the length of the sample, for different flow rates, at times for which  $u_{in} \cdot t$  is the same. If the flow front was fully saturated, flow front position would be at position  $x=u_{in} \cdot t / (1-V_f) = 0.05 \text{ m}$ . We observe that in all cases, as expected from the incomplete saturation,

the flow front has progressed further, and is the most spread when the flow rate is lower. From the value of saturation at the entrance of the preform, one can deduce the pressure inlet difference curves as a function of time, Fig. 9. The curves are initially not linear, and then become linear at time increases. Note that the shape of these curves is qualitatively similar to what is currently often observed experimentally, in Fig. 3 and in particular in Refs. [7-12].

When plotting the scaled pressure inlet curves  $P/u_{in}$  as a function of the delivered volume  $u_{in} \cdot t$ , Fig. 10, the curves all tend towards the same slope at long times. This slope corresponds to that found in the saturated case, where one would expect from Eq. (2) this curve to be a straight line, starting from 0 (chosen value of capillary pressure in this case), with a slope  $\eta/K/(1-V_f) = 2.5 \cdot 10^{10} \text{ Pa}$ . For high flow rates, the deviation from the linear curve is not very large, and a linear regression of the pressure curve would indeed lead to a capillary pressure value of 0, as chosen in the saturation curve Fig. 2. For low flow rates, however, the deviation is significant, and a linear regression would lead to erroneous values of the capillary pressure drop. Note that this is consistent with similar analysis performed in the case of infiltration of non-wetting fluids under constant pressure [26]. Note that the shape of the pressure inlet curve is function of the choice of the saturation curves: different fabric systems will lead to different saturation curves, hence to different pressure inlet curves, as observed experimentally in several references [7-12].

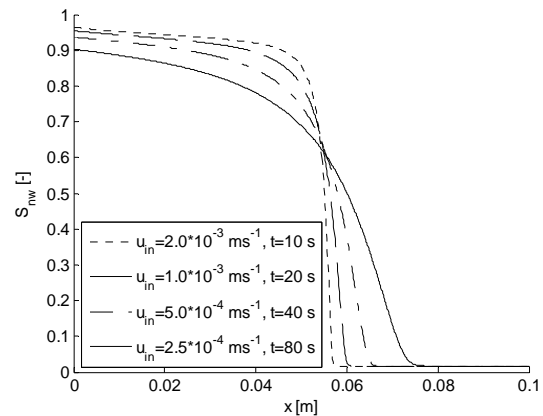


Fig. 8. Saturation curves at position  $u_{in} \cdot t$  for non-wetting resin for various injection velocities.

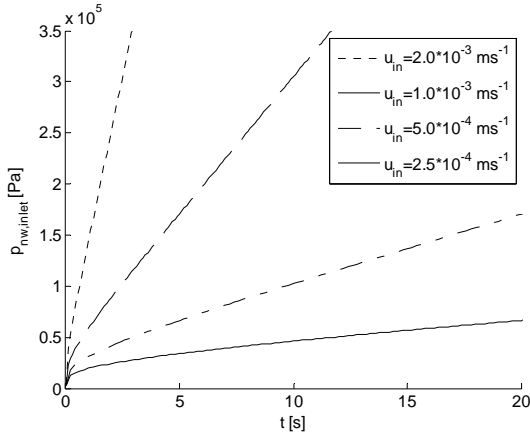


Fig. 9. Inlet pressure difference curves for injection of non-wetting resin at various injection velocities.

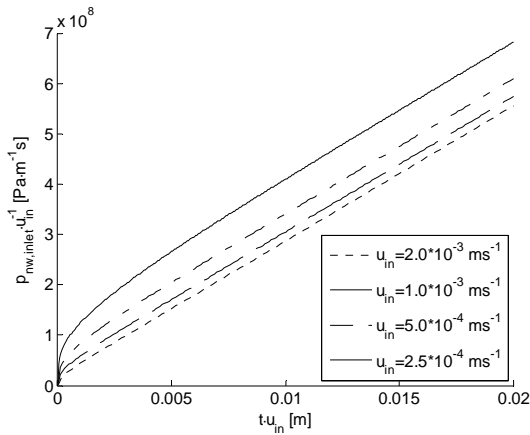


Fig. 10. Scaled inlet pressure difference curves vs. displaced fluid for injection of non-wetting resin at various injection velocities.

Similar results are found for the injection of wetting fluids. Fig. 11 shows the inlet pressure difference curve for a wetting resin, taking the saturation functions proposed in Fig. 3. The shape of the curves is similar, with a decreasing slope, and in that case, since we chose a threshold pressure head of  $H_b=5m$ , corresponding to a threshold pressure  $\Delta P_\gamma = -0.6 \cdot 10^5 \text{ Pa}$ , the curves start with a negative pressure difference at small times. Scaling these curves, as shown in Fig. 12, indicates that the lower the flow rate, the larger the deviation from the slug flow, as observed for the non-wetting case. For a high flow rate, the curve again tends towards the saturated curve. This curve shape is however not observed experimentally, as shown in

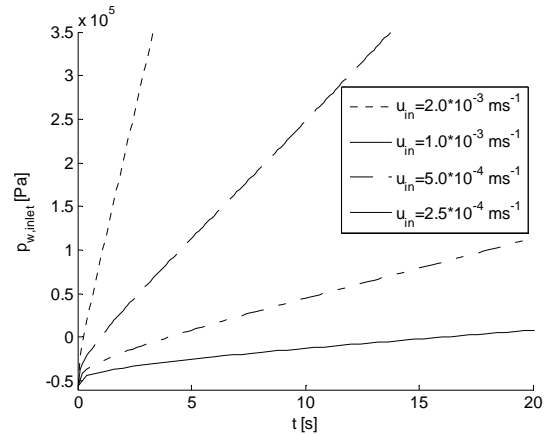


Fig. 11. Inlet pressure difference curves for injection of wetting resin at various injection velocities.

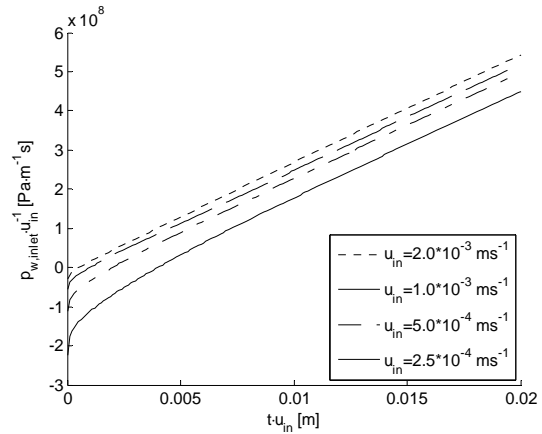


Fig. 12. Scaled inlet pressure difference curves vs. displaced fluid for injection of wetting resin at various injection velocities.

Fig. 5, and the discrepancy can find its origin in the experimental measurement of the inlet pressure curves. The pressure transducers used in this work could not register negative pressures and whenever the pressure was below 1 bar, the pressure transducers failed to register any increase in the inlet pressure. During this time, the inlet pressure difference appeared constant. Important information of the behaviour of the inlet pressure during injection may therefore have been left out in the experimental observations.

## 7 Conclusions

The present results show that a multiphase flow approach, based on the saturation concept as proposed in soil science provides numerical results that can describe the flow of resins in fibre preforms,

encountered in Liquid Moulding Processes. The pressure inlet curves for flow of a non-wetting fluid under constant flow-rate display the pressure slope decrease that is often observed in practice. For high flow rates, the error made in assuming a saturated flow becomes small; a value of a saturated capillary pressure drop can be measured with reasonable precision. The wetting case is also theoretically described by this method. In that case, however, the curves do not seem to match with experimental observations, most probably because of practical measurement issues which could be solved quite easily. It is worth noting, though, that wetting cases are generally found for low capillary numbers [4], implying that a saturated flow assumption will not be appropriate.

Finally, several hurdles need to be overcome to use this approach for a quantitative analysis of the experimental results: (i) the drainage-imbibition curves ( or saturation curves) for each fabric-resin system should be experimentally measured, (ii) dynamic effects on the magnitude of these curves should be estimated, (iii) the relative permeability change with saturation should also be quantified, possibly by inverse methods as done for soil science or metal infiltration [16]. These could first be addressed to set-up the experimental procedures with a Newtonian model fluid as proposed in Ref. [24], before investigating viscous curing resin systems.

### Acknowledgements

The authors thank SICOMP AB, Sweden and the Royal Swedish Academy of Sciences for financing part of the project. The results on carbon fabrics originate from the work of Dr J. Verrey at LTC, with funding from the EEC Growth project TECABS. Dr. A. Modaressi from Ecole Centrale Paris is also acknowledged for fruitful discussions.

### References

- [1] Michaud, V. and A. Mortensen, *Infiltration processing of fibres reinforced composites: governing phenomena*. Composites: Part A, **32**: p. 981-996, 2000.
- [2] Pillai, K.M. , *Modeling the unsaturated flow in liquid composite molding processes: A review and some thoughts*, Journal of composite materials, **38** (23): 2097-2118 2004.
- [3] Ruiz E, Achim V, Soukane S, et al., *Optimization of injection flow rate to minimize micro/macro-voids formation in resin transfer molded composites*, Composites Science and Technology 66 (3-4): 475-486 Mar 2006
- [4] Verrey, J., V. Michaud, and J.-A.E. Månson, *Dynamic capillary effects in liquid composite moulding with non-crimp fabrics*. Composites: Part A, **37**: p. 92-102, 2006..
- [5] Ahn, K.J., J.C. Seferis, and J.C. Berg, *Simultaneous measurements of permeability and capillary pressure of thermosetting matrices in woven fabric reinforcements*. Polymer Composites, 1991. **12**(3): p. 146-152.
- [6] Amico, S. and C. Lekakou, *An experimental study of the permeability and capillary pressure in resin-transfer moulding*. Composites Science and Technology, 2001. **61**: p. 1945-1959.
- [7] Babu, B.Z. and K.M. Pillai, *Experimental investigation of the effect of fibre architecture on the unsaturated flow in liquid composite moulding*. Journal of Composite Materials, 2004. **38**(1): p. 57-79.
- [8] Gourichon B, Binetruy C, Krawczak P, *Experimental investigation of high fiber tow count fabric unsaturation during RTM* , Composites Sci. and Tech. 66 (7-8): 976-982 Jun 2006
- [9] Parnas RS, Howard JG, Luce TL, et al., *Permeability characterization .1. A proposed standard reference fabric for permeability* , Polymer Composites 16 (6): 429-445 Dec 1995
- [10] Slade J, Pillai KM, Advani SG, *Investigation of unsaturated flow in woven, braided and stitched fiber mats during mold-filling in resin transfer molding* , Polymer Composites 22 (4): 491-505 AUG 2001
- [11] Pillai KM, Advani SG, *A model for unsaturated flow in woven fiber preforms during mold filling in resin transfer molding* , Journal of Composite Materials 32 (19): 1753-1783 1998
- [12] DeParseval Y, Pillai KM, Advani SG, *A simple model for the variation of permeability due to partial saturation in dual scale porous media* , Transport in Porous Media 27 (3): 243-264 Jun 1997.
- [13] Breard J, Henzel Y, Trochu F, et al. *Analysis of dynamic flows through porous media. Part I: Comparison between saturated and unsaturated flows in fibrous reinforcements* Polymer composites 24 (3): 391-408, Jun 2003.
- [14] Acheson JA, Simacek P, Advani SG, *The implications of fiber compaction and saturation on fully coupled VARTM simulation* , Composites Part A 35 (2): 159-169 2004
- [15] J.Wolfrath, V. Michaud, A. Modaressi and J.-A.E. Månson, *Unsaturated flow in compressible fiber preforms* , Composites Part A, 37, pp.881-889, 2006.
- [16] T. Dopler, A. Modaressi, V. Michaud, *Simulation of Metal Matrix Composite Isothermal Infiltration Processing*, Metallurgical and Materials Transactions B- 31 (2000) 225-234.
- [17] V. J. Michaud, L.M. Compton and A. Mortensen, *Capillarity in Isothermal Infiltration of Alumina Fiber*

- Preforms with Aluminium*, Metallurgical Transactions A, 25A, pp.2145-2152, october 1994.
- [18] Bear J, Bachmat, Y, *Introduction to modeling of transport phenomena in porous media*, Kluwer Academic Publishers, Dordrecht, 1991.
- [19] J. Bear, *Dynamics of Fluids in Porous Media*, American Elsevier, New York, 1972.
- [20] A. E. Scheidegger, *The Physics of Flow through Porous Media*, University of Toronto Press, Toronto, 1974.
- [21] R. A. Greenkorn, *Flow Phenomena in Porous Media*, Marcel Dekker, New York, 1983.
- [22] F. A. L. Dullien, *Porous Media, Fluid Transport and Pore Structure*, Academic Press, New York, 1979.
- [23] COMSOL AB, *Earth science module user's guide, Version 3.3*, August 2006.
- [24] Patel, N. and L. James Lee, *Modeling of void formation and removal in liquid composite molding. Part I. Wettability analysis*. Polymer Composites, 1996. **17**(1): p. 96-103.
- [25] Patel, N. and L. James Lee, *Modeling of void formation and removal in liquid composite molding. Part II. Model development and implementation*. Polymer Composites, 1996. **17**(1): p. 104-114.
- [26] V. Michaud and A.Mortensen, *On measuring wettability in infiltration processing*, Scripta Materialia, 56 (2007), pp.859-862.
- [27] COMSOL AB, COMSOL Multiphysics User's Guide, Version 3.3, August 2006.